Cyclic Peptides as Aggregation Inhibitors for Sickle Cell Disease

V. Neto[a], B. L. Victor [a], N. Galamba[a,*]

[a] Biosystems and Integrative Sciences Institute, Faculdade de Ciências da Universidade de Lisboa, Edifício C8, Campo Grande, 1749-016 Lisboa, Portugal

[*]Corresponding author: njgalamba@fc.ul.pt

Abstract

Sickle cell disease (SCD) is an autosomal recessive inherited disorder associated with a single substitution (Glu-β6→Val-β6) in the β-globins of the hemoglobin molecule. This replacement induces the aggregation of deoxygenated sickle cell hemoglobin (deoxy-HbS) into helical fibers that distort the red blood cells into a rigid sickle-like shape. Despite advances in stem cell and gene therapy as well as the recent approval of a new anti-sickling drug, therapeutic limitations subsist. Herein, we investigate, through molecular dynamics (MD), the effect of nine 5-mer cyclic peptides (CPs), tailor-designed to bind to the hydrophobic pocket or its surroundings, involved in key lateral contacts of HbS fibers. The size of the CPs was chosen to minimize proteolysis and favor cell penetration, while still allowing blocking the abovementioned region. Our results show that the CPs bind to the HbS pocket, orthogonally to the surface of the protein, with some revealing exceedingly long residence times. These CPs display a moderate to high specificity, exhibiting molecular recognition events in unbiased simulations, even at a HbS:CP (1:1) ratio. Further, hydration and binding free energies from alchemical and umbrella sampling MD indicate that all CPs should be soluble, although hydrophobic peptides are slightly self-aggregation prone. The respective CP-CP dimerization free energy is, nevertheless, higher (by a factor of ~ 6) than the HbS-CP binding free energy. A much lower (by a factor of ~ 6) HbS-CP binding free energy, longer residence times, and higher specificity are also found relative to a previously reported CP with modest *in vitro* antisickling activity. These results indicate that some of the CPs designed herein, namely, VVVVV and VFVFV (neutral), VEVFV (charge -1), VEVEV (charge -2), and VKVKV (charge +2) have the potential to reduce the concentration of aggregation-competent deoxy-HbS, by blocking or delaying the formation of the lateral contact at the homogeneous nucleation and/or fiber growth stages.

Introduction

SCD is a genetic disease associated with a missense mutation, namely, a single nucleotide change from A to T in the β-globin gene, resulting in the substitution of a glutamic acid (negatively charged) for a valine (neutral and hydrophobic) at the 6th position of the β-globins of normal adult hemoglobin, HbA[1–5]. This single replacement reduces the solubility[4] of deoxygenated sickle cell hemoglobin (deoxy-HbS), prompting the (reversible) aggregation of deoxy-HbS into 14-stranded helical fibers[4,6–15]. The latter distort the red blood cells into a non-deformable sickle-like shape, disrupting microcirculation, and ultimately resulting in hemolysis[16]. HbS fibers involve a lateral contact where Val-$\beta_2$6 has its hydrophobic side chain (isopropyl) lodged in a hydrophobic pocket of an adjacent HbS tetramer, formed by several hydrophobic residues, namely, Ala-$\beta_1$70, Phe-$\beta_1$85, and Leu-$\beta_1$88, as well as hydrophilic, Thr-$\beta_1$85 and Asp-$\beta_1$73[6–9,13], peripheral to the pocket (see **Fig. 1**). While the fibers also encompass axial (mutation unrelated) contacts, these are much weaker than the lateral contacts, likely responsible for triggering HbS nucleation[17–19].

Until recently, the only drug available targeting SCD was hydroxyurea (aka hydroxycarbamide), approved in the late 1990's[20], which increases the levels of fetal hemoglobin that does not polymerize, although several mechanisms of action (MOA) have been put forward[21]. More recently, two new drugs became available, namely, L-glutamine[22–25], whose MOA, although seemingly associated with a reduction of the oxidation stress, remains largely unknown, and voxelotor[26], an allosteric modulator aimed at stabilizing the nonpolymerizing relaxed form (R-state) of HbS (i.e., oxy-HbS). Nevertheless, these drugs have limitations regarding their efficacy[11,22,27]. For instance, Henry *et al*.[27] recently provided evidence that even though Voxelotor significantly reduces sickling, oxygen delivery to tissues is offset by increased hemoglobin O_2 affinity. On the other hand, although hematopoietic stem cell transplantation[28] and gene therapy[29] treatments can cure SCD, several challenges, including economic, persist, likely preventing these treatments' prevalence in a near future[10,11,30–32]. Thus, the development of a small molecule aggregation inhibitor capable of delaying or precluding the aggregation process remains of uttermost importance.

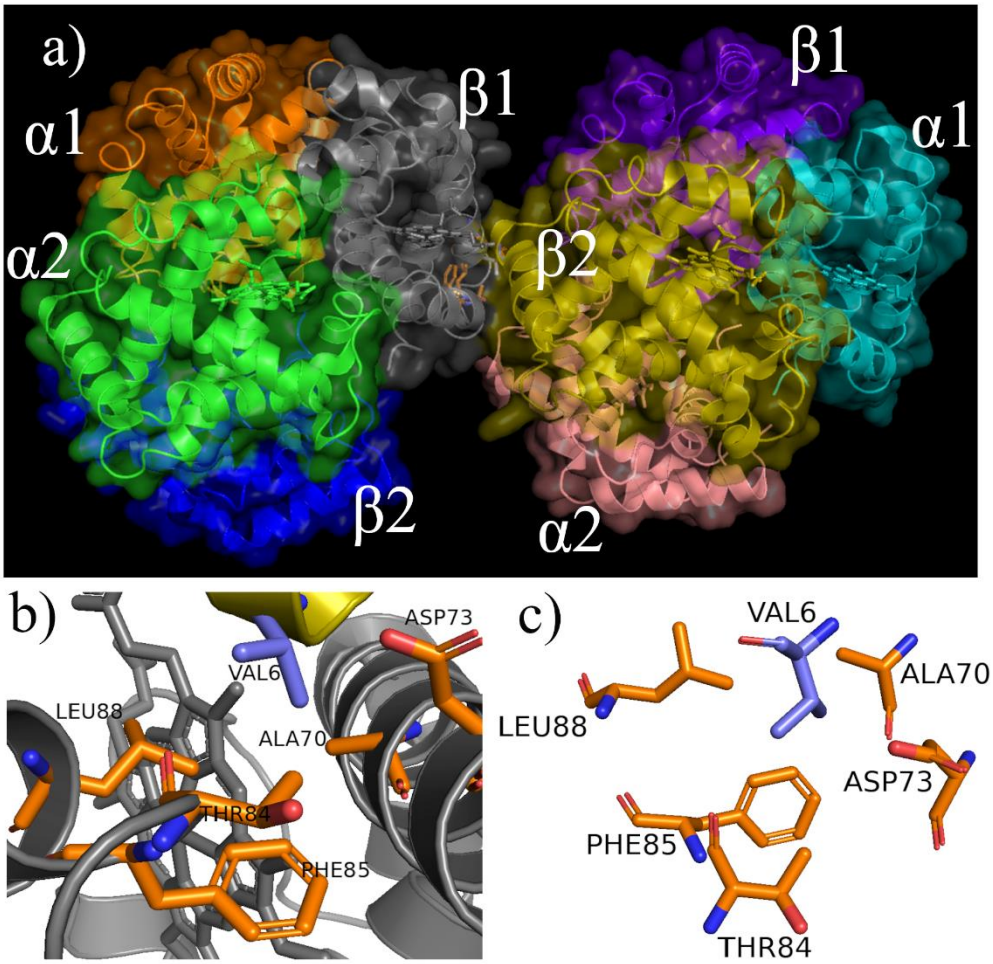

Figure 1 – **(a)** HbS dimer (pdb code: 2HBS)[7] showing Val-$\beta_2$6 on HbS-2 (right-hand side) lodged on the hydrophobic pocket of the HbS-1 molecule (left-hand side) of the dimer; **(b)** and **(c)** details of the pocket, including the **(c)** identity of the five closest amino acids to the Val-$\beta_2$6.

Over the years, several potential therapeutic strategies have been explored[10,11,31,33,34], namely, (i) the decrease of the intra-cellular HbS concentration, (ii) the decrease of the concentration of the allosteric effector, 2,3-diphosphoglycerate, increasing the solubility of HbS and destabilizing the fibers, (iii) the shift of the allosteric equilibrium toward the R-state, and (iv) the impediment of key protein-protein contacts in the fibers. Recently, a high-throughput assay encompassing 12,657 compounds of the Scripps ReFRAME drug repurposing library, was reported[35]. In this work, sickling times were assessed by following deoxygenation to 0% of red cells from sickle trait individuals. Metaferia *et al*.[35] found 106 compounds with antisickling activity, acting through some (unknown) of the abovementioned MOA. These small molecules, and other potential drugs with aggregation inhibitory properties have been recently reviewed in connection with aggregation inhibitors for neurodegenerative diseases[33].

The antisickling activity of amino acids and linear peptides were also long assessed[33,36–39]. An important conclusion from these studies was that peptides with multi-aromatic residues have a higher

activity than those that carry a single aromatic or aliphatic side chain. Peptide-based drugs constitute promising alternatives to small molecules as protein aggregation inhibitors because of their specificity and potency[40–44]. This enhanced potency is connected with a larger surface, allowing interacting with extended protein domains, pivotal to the aggregation process[42]. A downside of linear peptide drugs, however, concerns their low bioavailability and proteolytic stability[40,45]. Thus, in general, linear peptides are not viable drugs since proteolytic degradation precludes them from reaching the desired target at high enough concentrations. This has motivated the development of macrocyclic peptides and peptidomimetics, which can, in principle, overcome some of these limitations[40–45]. Nonetheless, cyclic peptides (CPs) have their own challenges, including possible self-aggregation propensity and cell membrane permeability limitations[44]. Following Dougherty *et al*., the vast majority of medium to large (i.e., > 5 amino acids) ring sizes have poor cell-permeability and oral bioavailability.[44] Amongst the reasons underpinning this low permeability are the large number of intrinsic hydrogen-bond (HB) donors (HBD) and acceptors (HBA), with each peptide bond contributing one HBD and two HBA, easily violating the "rule of five" that stablishes a maximum of 5 HBD and 10 HBA, for probable drug permeability.[46] The latter, however, can be reduced for small enough CPs forming intramolecular HBs, as observed in the CPs proposed in this work.

Some cyclic tetrapeptide homologs, namely, cyclo(-X-Glu[-Thr-Pro-]-OH; with X = Val or Phe) and cyclo(H-Thr-Pro-Val-Glu-OH), have been previously designed and synthetized to mimic the HbS mutation region, exhibiting, however, modest, or no *in vitro* antigelling activity[47]. Thus, the only cyclic tetrapeptide with some antigelling activity was cyclo(-Val-Glu[-Thr-Pro-]-OH), although its MOA could not be demonstrated. Among several possible factors, these results could be associated with a low specificity, as put forward by Sheh *et al*.[47].

Our main focus herein is on non-covalent stereospecific aggregation inhibitors, specifically, small, low molecular weight cyclic peptides (5 amino acids) able to block pivotal lateral protein-protein contacts, thus, potentially delaying or precluding stochastic homogenous nucleation and heterogeneous nucleation stages of HbS aggregation.[19,48,49] The free energy of dimerization of HbS was recently studied by one of the authors[50,51], showing that, in addition to the hydrophobic contact involving Val-$\beta_2$6 on a HbS-2 and the hydrophobic pocket on the β_1-globin of a HbS-1 tetramer, multiple salt bridges involving mainly Glu and Lys residues at the HbS-2 (α_2-globin and β_2-globin) and Lys, Glu, and Asp at the HbS-1 (β_1-globin) formed strong (electrostatic) contacts in the dimer arrangement. These results motivated herein the design of small CPs with the potential to bind either to the pocket or its surroundings, aiming at blocking pivotal protein-protein contacts. Additionally, a

4-mer CP with the same amino acids of the CP proposed by Sheh *et al*.[47] with a minor antigelling activity, was also studied for comparison purposes.

Methods

Molecular dynamics (MD) of a deoxy-HbS monomer in 0.1 M NaCl aqueous solutions with and without different CPs, were performed at 310 K and 0.1 MPa. HbS (as HbA) is composed of four polypeptide chains, 2 α subunits (α-globin) and 2 β subunits (β-globin). Each α-globin is formed by 141 amino acids and a Heme group whereas each β-globin is formed by 146 amino acids and a Heme group. The structure of the first HbS (HbS-1) in the dimer (pdb code[7]: 2HBS) was used to generate the starting configurations of each system (see **Fig. 1**). The HbS and CPs were modelled with the CHARMM36 force field whereas water was described by the mTIP3P (i.e., CHARMM modified TIP3P) model[52,53]. Although the original TIP3P model[54] was used to optimize the CHARMM36 force field, the mTIP3P was preferred since this model is used to simulate membranes with CHARMM, also being investigated in our group, specifically, membrane bilayer drug permeability. These models differ only in that mTIP3P H atoms have Lennard-Jones interactions, opposite to the TIP3P. The mTIP3P water has a higher density and a slightly slower dynamics compared to the TIP3P model (see **Table S1**). Nevertheless, simulations herein with both models showed no major structural differences in the HbS monomer (see **Fig. S1**), opposite to a previous study, although for peptide folding[55]. MD of a monomer of deoxy-HbA (pdb code[56]: 2DN2) was also performed for comparison purposes concerning the hydrophobic pocket, common to both HbA and HbS.

The following nine 5-mer synthetic CPs were studied: VVVVV, VFVFV, VEVFV, VEVEV, VEVDV, VDVDV, VDVKV, VKVKV, and DDDDD (see **Fig. 2**). The size (i.e., 5 residues) of the CPs was chosen to be sufficiently small to potentially resist to proteolytic degradation and facilitate membrane permeability[44], while large enough to block the hydrophobic pocket in the β_1-globin where the Val-$\beta_2$6 of a neighbor HbS is lodged (see **Fig. 1**) and/or some nearby region. Notice that some CPs have charge +2, -2, and -5, potentially perturbing their membrane permeation capabilities. These charged peptides were designed to assess the effect of electrostatic interactions concerning protein-CP recognition, in particular, the potential formation of salt bridges with amino acids near the pocket[50,51]. The permeation across an erythrocyte membrane model will be the focus of future work.

For each structure, a geometry optimization and frequency calculation was performed at the DFT/B3LYP[57,58] level with a 6-31+G(d,p) basis set with the program Gaussian 16[59]. A local minimum (see **Fig. 2**) was found for all the CPs showing that the CPs have no steric clashes, forming one to two backbone HBs[60]. These conformations were used as the starting configurations for each

MD simulation.

The choice of the amino acids was based on the abovementioned previous studies[50,51] and the pocket nature. A VVVVV CP is expected to bind to the hydrophobic pocket, and was, therefore, the basis for designing the CPs, with the exception of one (i.e., DDDDD). Thus, seven CPs were designed based on the replacement of two alternating Val residues by Glu, Phe, Asp, and/or Lys. The choice of Phe was related with the presence of Phe85 in the pocket, thus, potentially allowing establishing π-stacking interactions, and the fact that several drugs found to inhibit protein aggregation, including HbS[33,36], have aromatic rings. Glu and Asp were chosen under the premise that these amino acids could hinder aggregation by destabilizing protein-protein salt bridges next to the pocket, whereas Lys was chosen because it can form a salt bridge with Asp73 in the pocket (see **Fig. 1**). The ninth peptide was chosen to be DDDDD as a model of a fully hydrophilic, highly charged CP, with the potential to destabilize protein-protein salt bridges next to the pocket, but possibly not binding to the pocket. The peptides were cyclized through addition of a covalent bond between the C- and N- termini; thus, except for DDDDD this bond was formed between the C- and N- termini of Val amino acids (see **Fig. 2**).

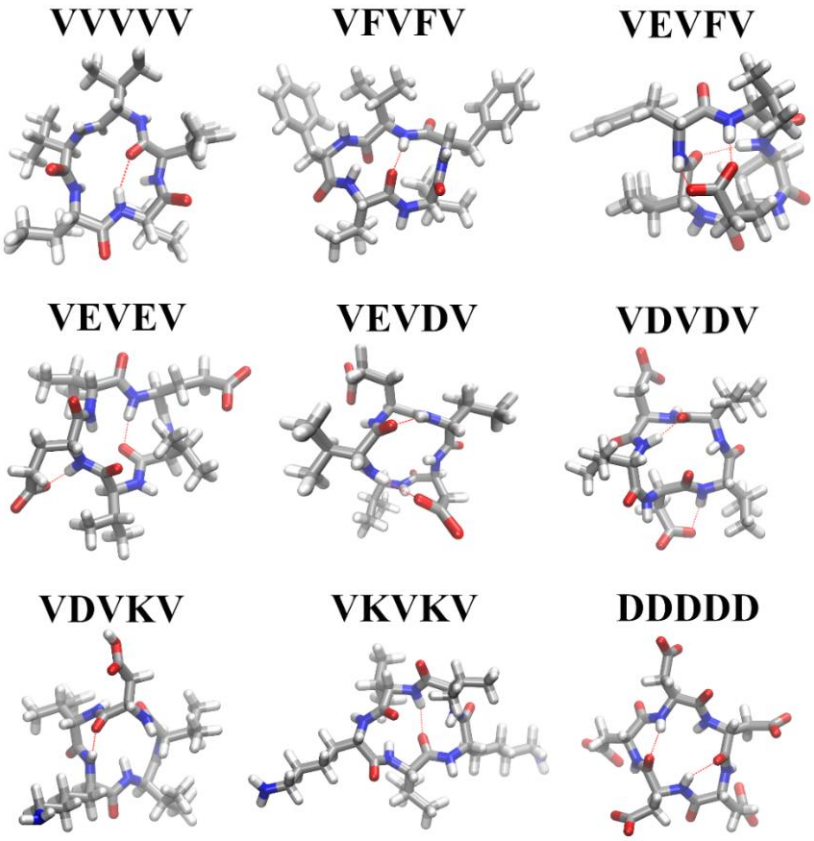

Figure 2 – Density functional theory B3LYP/6-31+G(d,p) local minima for the different CPs. VVVVV, VFVFV, and VDVKV (zwitterionic) are neutral, VEVFV has charge -1, VEVEV, VEVDV, and VDVDV have charge -2, VKVKV has charge +2, and DDDDD has charge -5.

Additionally, a 4-mer peptide, VETP, which shares the same four amino acids with the CP proposed by Sheh *et al.*[47], and that exhibited some, although low, antigelling activity *in vitro*, was studied; this peptide was cyclized the same way as the 5-mer peptides.

We performed a set of MD simulations of HbS with a single CP, where the starting configuration was one where the CP was placed near the hydrophobic pocket of an HbS monomer. A set of three distinct protein-CP starting configurations (SC), two with the CPs oriented parallel (SC1 and SC2) and one orthogonal to the pocket (SC3), were built. These starting configurations were used to perform 5 to 10 replicas, for each CP, starting with different velocities. The HbS was placed in a cubic box (9.0, 9.0, 9.0 nm) corresponding to a distance of 1.7 nm between the protein and its nearest images and solvated by over 20 000 water molecules and Na^+ and Cl^- ions (0.1 M NaCl).

Following a steepest descent energy minimization and a 50 ps MD in the *NVT* ensemble, the systems were equilibrated in the *NpT* ensemble for 50 ns. HbS and the CPs were restrained during this equilibration period. The *T* and *p* were controlled with the thermostat of Bussi *et al.*[61] and the Parrinello-Rahman barostat[62]. Electrostatic interactions were computed via the particle-mesh Ewald (PME) method[63]. A cut-off of 1 nm was used for non-bonded van der Waals and for the PME real space electrostatic interactions. The equations of motion were solved with the Verlet leap-frog algorithm with a 2 fs time-step for VVVVV and VFVFV and a 1 fs time-step for the remaining (charged) CPs. The trajectories were propagated in 50 ns blocks until the CPs departed from the pocket or up to a maximum of 150 ns. Some trajectories for some CPs were then further propagated up to 500 ns.

A second and third sets of MD simulations with a single and five CPs, respectively, randomly inserted in an aqueous solution of the HbS, were carried out. A similar approach as the one previously described was followed, with the exception that no harmonic restraints were imposed during equilibration. The trajectories were propagated for 500 ns and three replicas were performed for each set of MD simulations.

The first set of MDs aimed at probing the CPs residence time in the pocket, whereas the second and third probed the CPs' specificity for the pocket and other regions of the HbS.

The pocket in both β-globins of HbS and HbA was characterized by the solvent accessible surface area (SASA). We assessed the SASA for three pocket definitions for comparison purposes: pocket-3aa (Ala70, Phe85, Leu88), pocket-4aa (Ala70, Thr84, Phe85, Leu88), and pocket-5aa (Ala70, Asp73, Thr84, Phe85, Leu88) (see **Fig. 1(c)**). The remaining analyses considered the pocket formed by the five amino acids (i.e., pocket-5aa).

We also calculated the potential of mean force (PMF) (i.e., aggregation free energy profile) of the

VVVVV and VFVFV CPs and the hydration free energy of VVVVV, the most hydrophobic CP amongst those studied. Additionally, the HbS-CP PMF was calculated for VVVVV, VEVFV, and VETP, to assess the receptor-ligand binding free energy. The PMFs[64,65] were computed through umbrella sampling[66–68]. The reaction coordinate, ξ, was chosen to be the distance between the COM of the CPs and between the HbS pocket and the CP. A spacing of 0.05 nm and a spring constant of 1000 $kJmol^{-1}nm^{-2}$ for the harmonic potential were used. The umbrella sampling MD were performed for 50 ns after steepest descent energy minimization, a 100 ps equilibration in the *NVT* ensemble, and 15 ns equilibration in the *NpT* ensemble. The PMFs were obtained through the weighted histogram analysis method[69,70] and corrected for the entropy[71] by adding the Jacobian correction factor $2RT\ln(\xi)$, associated with the increasing sampling volume with the ξ increase[72]. The Bayesian bootstrap method[73] was used to estimate the PMFs errors. The PMFs were shifted to have zero free energy at large separation distances. The error associated with the volume overcorrection of the HbS-CP PMF due to protein steric hindrance was estimated to be of the same order of magnitude as the PMF bootstrap error.

The hydration free energy of VVVVV was calculated through "alchemical" free energy simulations with the Bennett acceptance ratio method[74]. The ΔG_{hyd} was obtained from two replicas with 20 λs and 20 ns, and 40 ns trajectories, respectively, for comparison purposes. Further details on the PMF and hydration free energy calculations are available elsewhere[75,76].

Results and Discussion

CP-HbS Pocket Residence Time

We begin our discussion by analyzing the trajectories for which the starting configurations comprised a single CP placed next to the hydrophobic pocket of an HbS monomer, followed by steepest descent energy minimization in aqueous solution (see **Methods** section). **Figure 3** shows the time evolution of the minimum distance, d_{min}, between the CPs and the pocket atoms, for five trajectories. For all but DDDDD the CPs remained in the pocket for 50 ns and all but DDDDD, VEVDV, and VDVKV, remained in the pocket for 150 ns, in at least one trajectory. The CP DDDDD migrated readily to a region 5-10 Å away from the interior of the pocket, where it stayed for at least 50 ns in more than one trajectory. This indicates the inability of a CP without at least a hydrophobic amino acid to remain lodged in the interior of the pocket. On the other hand, it supports the view that hydrophilic amino acids in the HbS lateral contact can bind to charged groups in the CPs. Thus, DDDDD was found to interact with Thr84 which is enclosed in our pocket-5aa definition (see **Methods** section). Nonetheless, given the high negative overall charge of this CP, the trajectories

were not further extended, since this peptide is unlikely to have a good selectivity and membrane permeability (not studied here).

We also assessed the residence time with TIP3P water model, and a seemingly similar behavior was observed (see **Fig. S2**), despite potential differences associated with the solvent are difficult to probe.

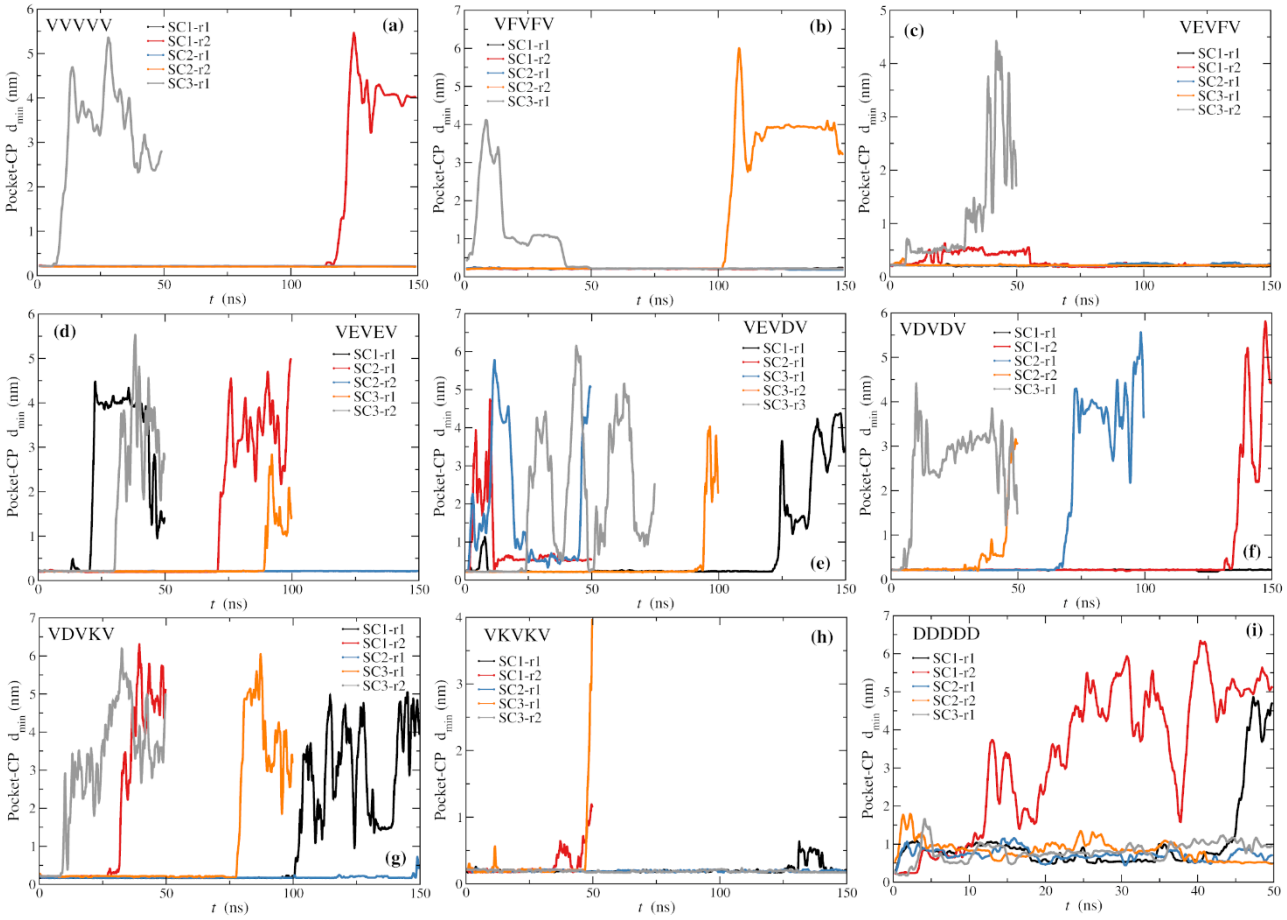

Figure 3 – Moving averages of the time evolution of the minimum distance between the CPs and the pocket up to a maximum residence time of 150 ns. SC stands for starting conformation (HbS-CP) and r stands for replicate. Five representative replicates are shown for each CP. The DDDDD CP leaves the interior of the pocket binding to Thr84 (also part of the pocket definition) and nearby amino acids.

The above residence times were found to be easily reproduced for some CPs and starting configurations. We stress that while the term residence time is used here regarding specific trajectory observations, our simulations do not involve enough replicates, nor long enough simulation times to accurately estimate an average residence time (τ_R). The binding kinetics, characterized by the association (k_{on}) and dissociation (k_{off}) rate constants (k_{off} is related to the residence time by $\tau_R = 1/k_{off}$) provides a measure of drug efficacy and is at least as important as the binding affinity, commonly quantified by the equilibrium dissociation constant (K_d) or the half-maximal inhibitory concentration (IC_{50})[77–80].

The peptides that consistently remained in the pocket over the different replicas and exhibited the longest residence times were: VVVVV and VFVFV (neutral), VEVFV (charge -1), and VKVKV (charge +2). Although only 5 trajectories are shown (for sake of clarity), additional trajectories showed a similar behavior, including residence times of 150 ns for the latter peptides. Moreover, VVVVV, VFVFV, VEVFV, and VEVEV, remained in the pocket up to 500 ns in at least one trajectory (see **Fig. S3**).

All CPs oriented (in average) orthogonally to the protein surface, and therefore, to the pocket, independently of the starting configuration, pointing one to two amino acid side chains to the pocket (generally a single Val) while the remaining side chains interacted with pocket-neighbor amino acids or protruded to the solvent (see **Fig. 4**).

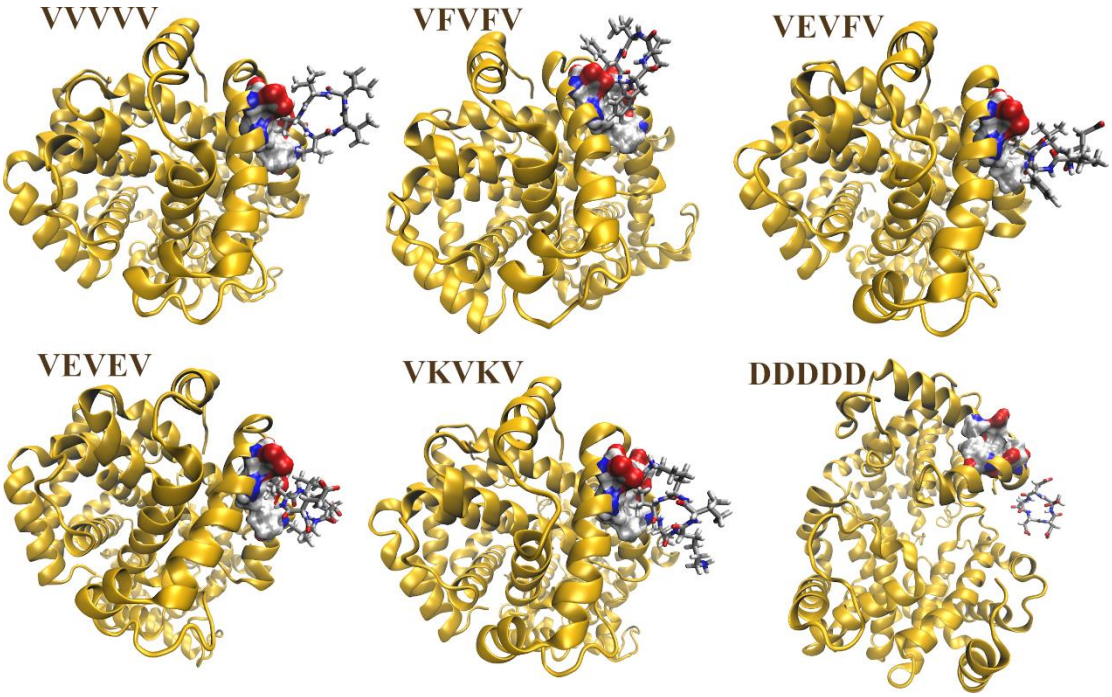

Figure 4 – Representative configurations illustrating the relative orientation of the CPs with longer residence times in the HbS pocket, VVVVV, VFVFV, VEVFV, VEVEV, and VKVKV, and DDDDD (not in the interior of the pocket – see **Fig. 3**). The remaining CPs also oriented orthogonally to the pocket.

CP-HbS Specificity

An inherent difficulty in the development of aggregation inhibitors targeting the hydrophobic pocket is the fact that each HbS molecule has two hydrophobic pockets whereas a single pocket is involved in the lateral contacts of the fibers. Thus, while similar pockets are located at the β_1-globin and β_2-globin, the lateral contact in the HbS fibers involves the β_1-globin and the β_2-Val6 of a neighbor HbS. We have assessed the solvent accessible surface area (SASA) of the hydrophobic

pocket in both β-globins of HbS and HbA. **Figure S4** shows that the SASA is similar amongst the β-globins on both HbS and HbA. Hence, in addition to the large concentration of HbS in the erythrocytes, the existence of two similar pockets indicates that a large concentration of a drug acting through this MOA may be necessary to be effective.

Nevertheless, given the large dependence of the kinetics of aggregation on the concentration of HbS and the fact that only deoxy-HbS aggregates, a small decrease of the concentration of aggregation-competent HbS (i.e., "pocket-free" HbS) could result in a significant sickling reduction[4,10]. Additionally, a drug may also inhibit aggregation by binding to the mutation site, that is, Val-$\beta_2$6. As we shall see, the most effective CPs studied here also display some affinity toward Val-$\beta_2$6.

A second, related difficulty, concerns drug specificity, that is, the drug's ability to bind to the pocket while bearing a low affinity toward other protein domains.

Unbiased MD can provide insight into pocket specificity, in spite of sampling limitations. Here we performed three MD replicas, 500 ns long, for a monomer of HbS with either one or five CP molecules. The use of five CPs increases not only the probability of observing HbS pocket-CP binding but also to other additional (undesirable) pockets which may sequestrate the CPs.

Our results show that those peptides that exhibited longer residence times also demonstrated a higher specificity.

Figure 5 displays contact maps for the HbS:CP (1:1) systems for the five CPs with longer τ_R. A similar plot for HbS:CP (1:5) is displayed in **Fig. 6**. The maps were computed by averaging the number of CP-protein contacts over the different MD replicas. A protein-CP contact is defined by the protein-CP minimum distance, R_{min}, with $R_{min} < 3.5$ Å, where R_{min} is assessed by probing the atomic distances between every atom of the protein and every atom of the CP. The number of contacts, N_c, was normalized by the maximum number of protein-CP contacts across every CP, $N_{c,max}$.

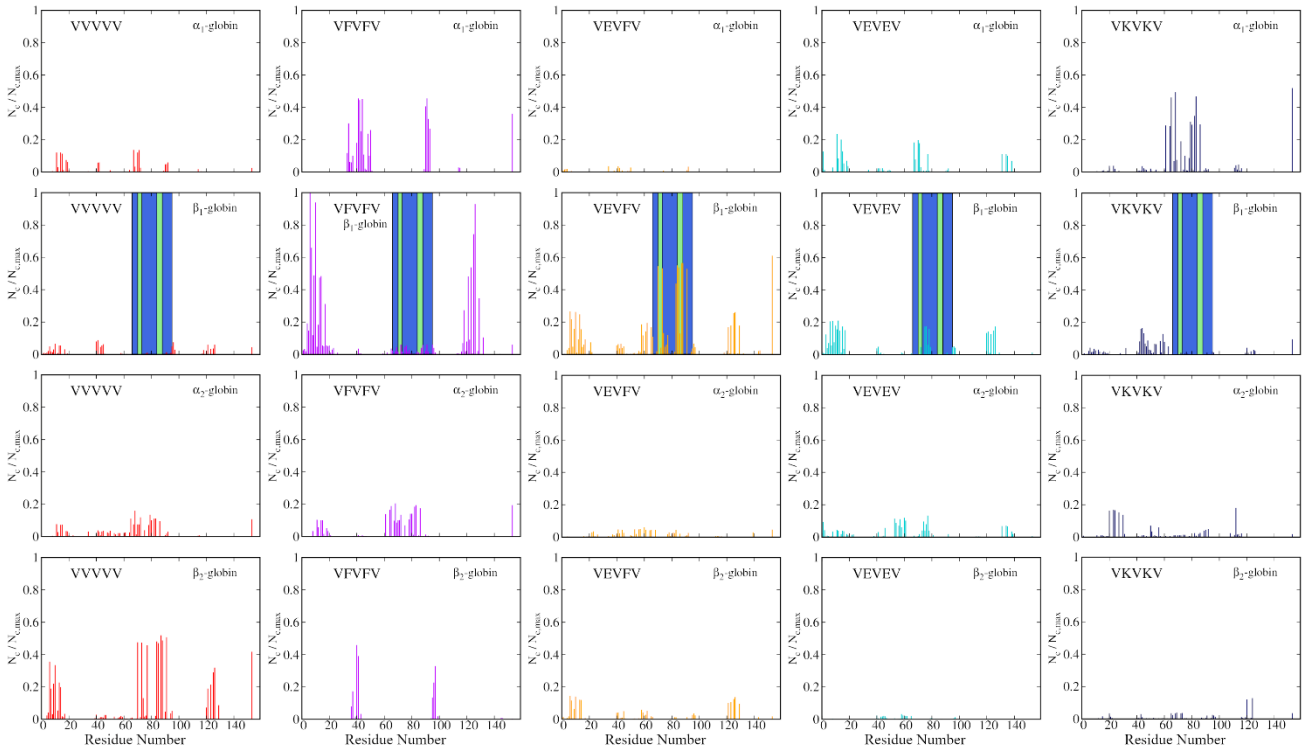

Figure 5 – Normalized HbS-CP contact maps for the HbS:CP (1:1) systems with highest residence times. Notice that whereas VVVVV does not exhibit contacts with the β_1-pocket it does have a large number of contacts with the equivalent pocket in the β_2-globin (see **Fig. S4**).

For the HbS:CP (1:1) systems $N_{c,max}$ was observed for VFVFV whereas for the HbS:CP (1:5) this was found in VEVFV, both, in the β_1-globin, *albeit* not in the pocket. Whereas the above cut-off (i.e., $R_{min} < 3.5$ Å) is somewhat arbitrary, qualitatively similar results were obtained using a larger distance $R_{min} < 4.5$ Å (see **Fig. S5**).

The vertical green stripes in **Figs 5** and **6** denote the pocket in the β_1-globin whereas the peripheral blue stripes enclose the remaining amino acids involved in the lateral contact in the HbS dimer. The latter were defined as the residues of the HbS-1 monomer at a distance of less than 4.0 Å from any residue of the HbS-2 monomer in the crystal structure of the HbS dimer (pdb code: 2HBS)[7]; the distances were computed between every atom in the monomers.

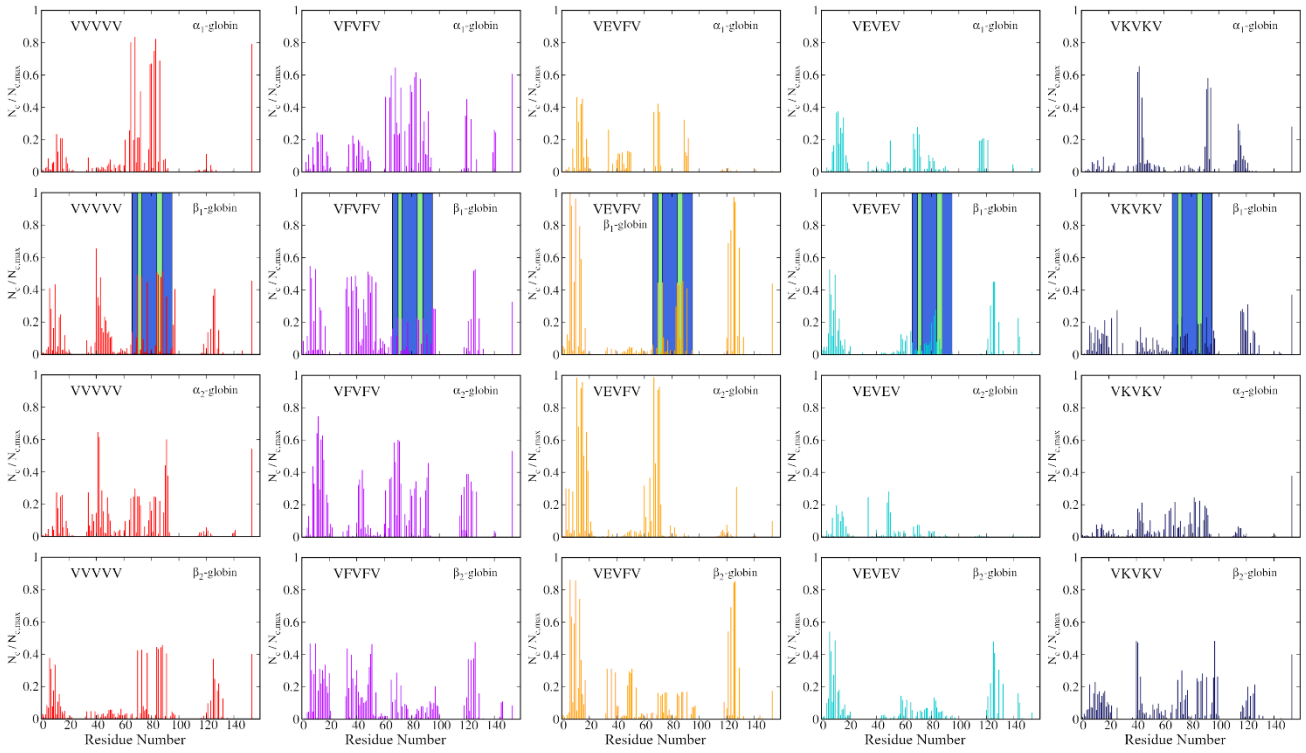

Figure 6 – Normalized HbS-CP contact maps for the HbS:CP (1:5) systems with highest residence times and specificity.

The largest number of contacts in the β_1-globin is observed for VEVFV amongst the HbS:CP (1:1) systems. For VVVVV a large number of contacts with the equivalent pocket in the β_2-globin is also observed.

A similar picture is found for the HbS:CP (1:5) systems. Additionally, VEVEV exhibits the lowest number of contacts with the protein, independent of the chain, meaning that this CP remains in the solvent more time than the remaining CPs.

Although not the intended primary target of the CPs, it can also be seen that VVVVV interacts with the mutated amino acid (i.e., Val-$\beta_2$6) in HbS:CP (1:1), whereas for HbS:CP (1:5) all CPs interact with this region. However, a large number of contacts is also observed in other domains of every polypeptide chain. **Figures 5** and **6** also show that the CPs interact with the Hem group (residue 153 in α and β chains as in the original pdb 2HBS[7]). Whether these interactions influence HbS allostery, either favoring the R or T states was not assessed here.

To gain further insight into the CPs specificity, namely, to disentangle between short-time and long-time contacts with each pocket, we also assessed the minimum distance along time between the β_1-globin and β_2-globin pockets and the CPs. These are displayed in **Figure 7** for two out of the three trajectories (for clarity) with one and five CPs. Notice the distance between the pockets in β_1-globin and β_2-globin is ~2-2.5 nm. This can be readily seen by comparing the CPs' distances to the β_1-

globin and β_2-globin pockets in the HbS:CP (1:1) ratio plots when the single CP is lodged in one of the pockets ($d_{min} < \sim 0.5$ nm).

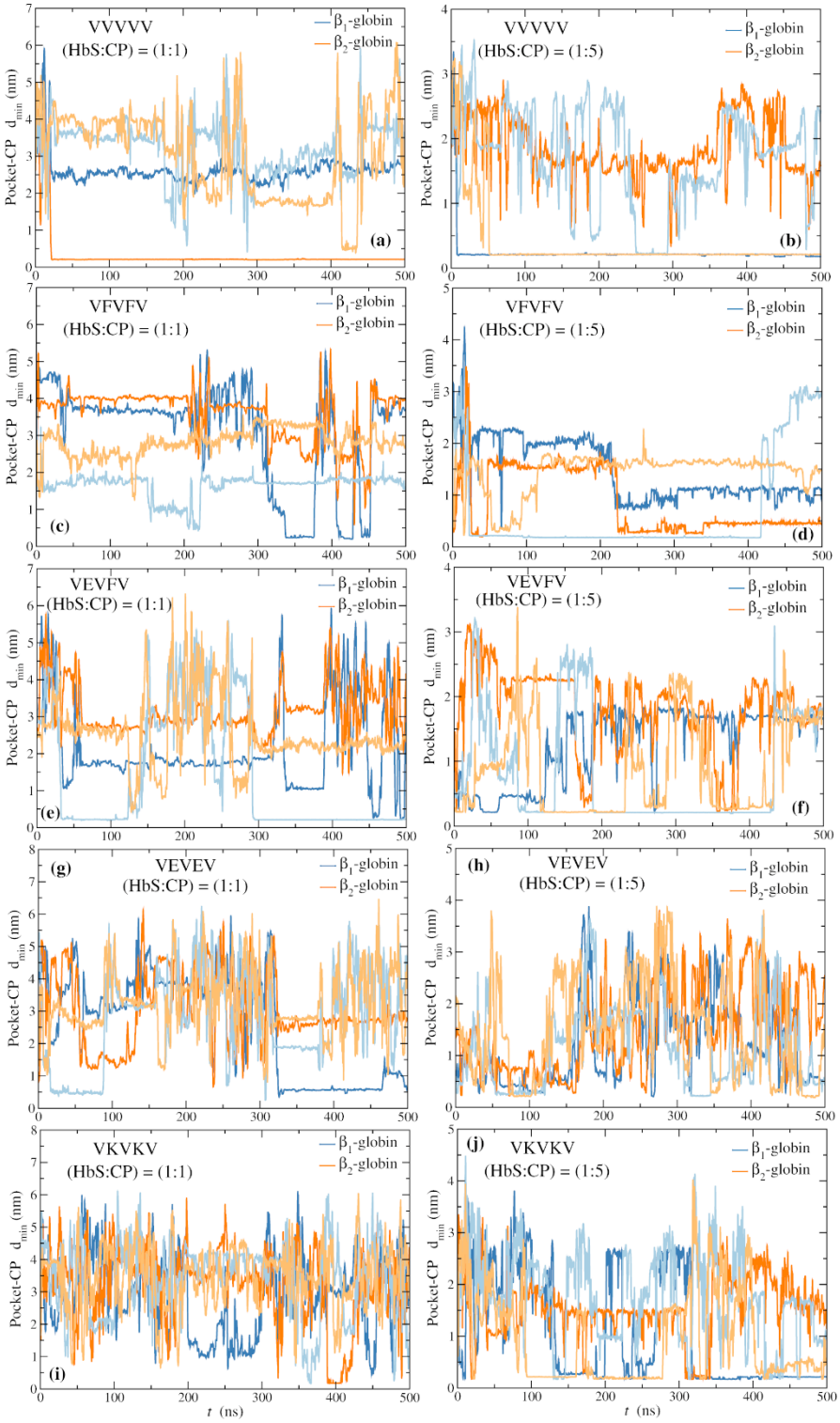

Figure 7 – Moving averages of the time evolution of the minimum distance between the CPs and the β_1 and β_2-globin pockets from MD simulations where the CPs are randomly inserted in solution at time zero. Dark (replica 1) and light (replica 2) blue curves are the distances to the β_1-globin pocket (where Val 6 is lodged in HbS fibers) and dark (replica 1) and light orange (replica 2) are the distances to the β_2-globin pocket.

Figure 7 shows that the CPs bind to the pocket within timeframes that range between a few ns to hundreds of ns, even for a HbS:CP (1:1) ratio. The longest residence times are found for VVVVV, although dissociation is not observed within the trajectory timeframe for several CPs, precluding the determination of τ_R. Nevertheless, the fact that the CPs interact with the pocket (often multiple times) in an unbiased MD within a timeframe of 0.5 μs, suggests the peptides have at least, a moderate to high specificity.

Notice the peptides are ought to bind deoxy-HbS which can be considered a short-lived receptor due to the allosteric equilibrium. Thus, a fast-binding drug is important to reduce the concentration of deoxy-HbS aggregation-competent, whereas long residence times may not be critical. These timescales (millisecond) are, however, significantly longer than those studied herein. **Figure 7** also suggests the CPs can associate and dissociate multiple times during those timescales.

From a binding mechanism point of view, observation of the MD trajectories, suggests that CP-pocket (Ligand-Receptor) binding undergoes a two-state association/dissociation mechanism, $R + L \underset{k_{off}}{\overset{k_{on}}{\rightleftarrows}} = RL$. Additionally, it was observed that the "limiting-step" underlying many CP-pocket frustrated contacts (i.e., not resulting in lasting binding; see **Fig. 7**) results from a non-optimal orientation approach (i.e., non-orthogonal to the protein surface). CP orientation towards the binding of the pocket seems, therefore, pivotal to crossing the transition state barrier and *a posteriori* stabilization of the bound state.

CPs' Solvation and Aggregation

Another key aspect of any drug concerns its solubility in water, which is closely related with the hydration free energy and the drug's aggregation propensity. The hydration free energy of VVVVV, the most hydrophobic CP studied here, was estimated to be ΔG_{hyd} = -106 kJ mol^{-1} (replica 1: ΔG_{hyd} = -103 kJ mol^{-1}; replica 2: ΔG_{hyd} = -108 kJ mol^{-1}). The ΔG_{hyd} of the remaining CPs should be significantly lower, suggesting that all the CPs are soluble in water.

We also assessed the potential of mean force (PMF) (i.e., dimerization free energy profile) of VVVVV and VFVFV (see **Fig. 8(a)**) to evaluate their aggregation propensity. The peptides exhibit a mild tendency to aggregate exhibiting a well-defined contact pair and solvent separated minima around -5±2.5 kJ/mol. The remaining CPs that displayed high residence times next to the pocket are charged and have, therefore, a repulsive free energy profile.

The protein pocket-CP binding free energy was also assessed for VVVVV to evaluate its magnitude relative to its dimerization free energy (see **Fig. 8(b)**).

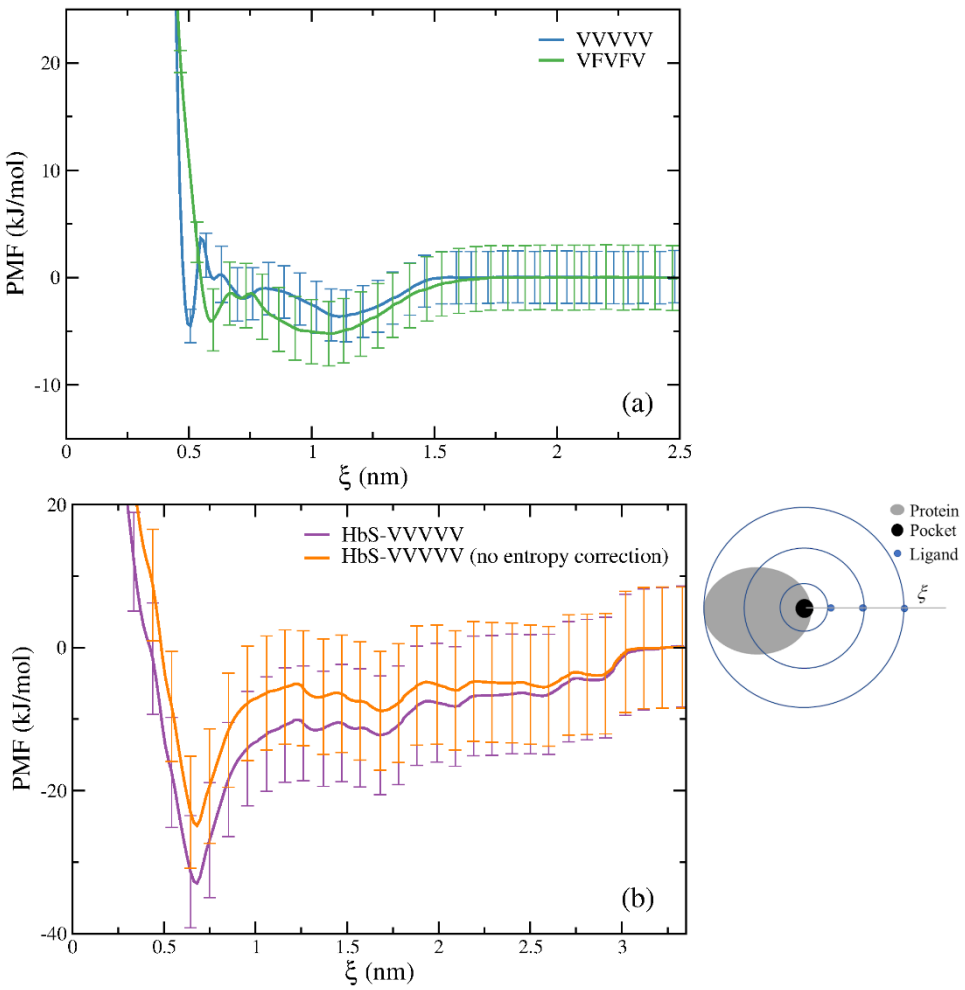

Figure 8 – Potential of mean force (PMF) for **(a)** the dimers of VVVVV and VFVFV and **(b)** HbS and VVVVV in water at 310 K and 0.1 MPa. The right-hand-side of **(b)** shows a 2-dimensional representation of HbS and the CP radial space allowed at three distinct values of ξ. As ξ increases the fraction of impeded volume decreases being zero at ξ equal to the largest diameter of the HbS, approximated by a spheroid.

A binding free energy around -17±6.0 kJ/mol was found, thus ~3 times lower than the CP-CP binding free energy; the error was estimated from error propagation of the bootstrap errors at the minimum and long distances when the shifted PMF is zero. To assess the maximum error associated with the Jacobian overcorrection due to protein steric hindrance (i.e., the interception of the circles and the spheroid in the right-hand-side scheme of **Fig. 8(b)**) the PMF was calculated without the Jacobian correction, resulting in a binding free energy of -10±6.0 kJ/mol. This is possible because the uncorrected PMF still converges to a plateau. This difference is of the same order of magnitude of the bootstrap error.

To allow for an easy comparison between the distinct CPs as potential HbS aggregation inhibitors we ranked our results based on a simple (arbitrary) classification of the different parameters assessed in this work (see **Table 1)**.

Table 1 – CPs classification based on the residence time (τ_R) of the CPs next to the pocket, pocket specificity, and self-aggregation propensity.

CP	Charge	τ_R [a]	Specificity[b]	Self-aggregation
VVVVV	Neutral	High	High	Moderate
VFVFV	Neutral	High	Moderate-High	Moderate
VEVFV	-1	High	High	No
VEVEV	-2	Moderate	Moderate-High	No
VEVDV	-2	Low	Moderate	No
VDVDV	-2	Moderate	Low	No
VKVDV	Zwitterionic	Moderate	Low	No
VKVKV	+2	High	Moderate	No
DDDDD	-5	n/a[c]	High[d]	No

[a] High: $R_t \geq 150$ ns in more than half of the trajectories; Moderate: $R_t < 150$ ns in more than half of the trajectories; Low: $R_t < 150$ns for all trajectories.

[b] High: The CP binds to either pocket for at least one trajectory in a HbS:CP (1:1) ratio; Moderate: The CP binds to either pocket for at least one trajectory in a 1:5 HbS:CP ratio but not at a HbS:CP (1:1) ratio; Low: The CP does not bind to either pocket at either HbS:CP ratio.

[c] DDDDD binds to a region close to the pocket; however, because of its high charge it was not further investigated.

[d] DDDDD has a high specificity for the region close to the pocket anchored by Thr84.

Thus, according to this classification, VVVVV, VFVFV, VEVFV and to a less extent VEVEV and VKVKV display the most promising results. From these CPs VEVFV seems to be the CP with the most promising HbS aggregation inhibition characteristics. Future studies should assess membrane permeability of these CPs as well as their potential influence on the HbS allostery equilibrium.

Previously Reported Antisickling Cyclic Peptides

To make contact with the CPs proposed by Sheh *et al.*[47] a 4-mer CP, VETP, was also studied. This peptide has the same amino acid sequence as the only CP with reported *in vitro* antisickling activity, amongst those proposed by Sheh *et al.*[47]. **Figure 9(a)** shows the optimized geometry of the CP obtained through DFT B3LYP/6-31+G(d,p), displaying a single backbone HB. Opposite to most CPs proposed in our work, VETP exhibits relatively short residence times (see **Fig. 9(b)**). Thus, although a similar orthogonal orientation was observed (**Fig. 9(c)**), with the Val side chain lodged in the pocket, the peptide did not persist up to 150 ns in none of the trajectories, independent of the starting conformation. Fifteen trajectories were propagated with a time-step of 1 fs, starting from the same starting conformations used for the other CPs. Furthermore, analysis of the pocket-VETP minimum distances in a solution with 5 CPs shows this peptide has a low specificity, never binding to the

pocket in a lasting way (see **Fig. 9(d)**).

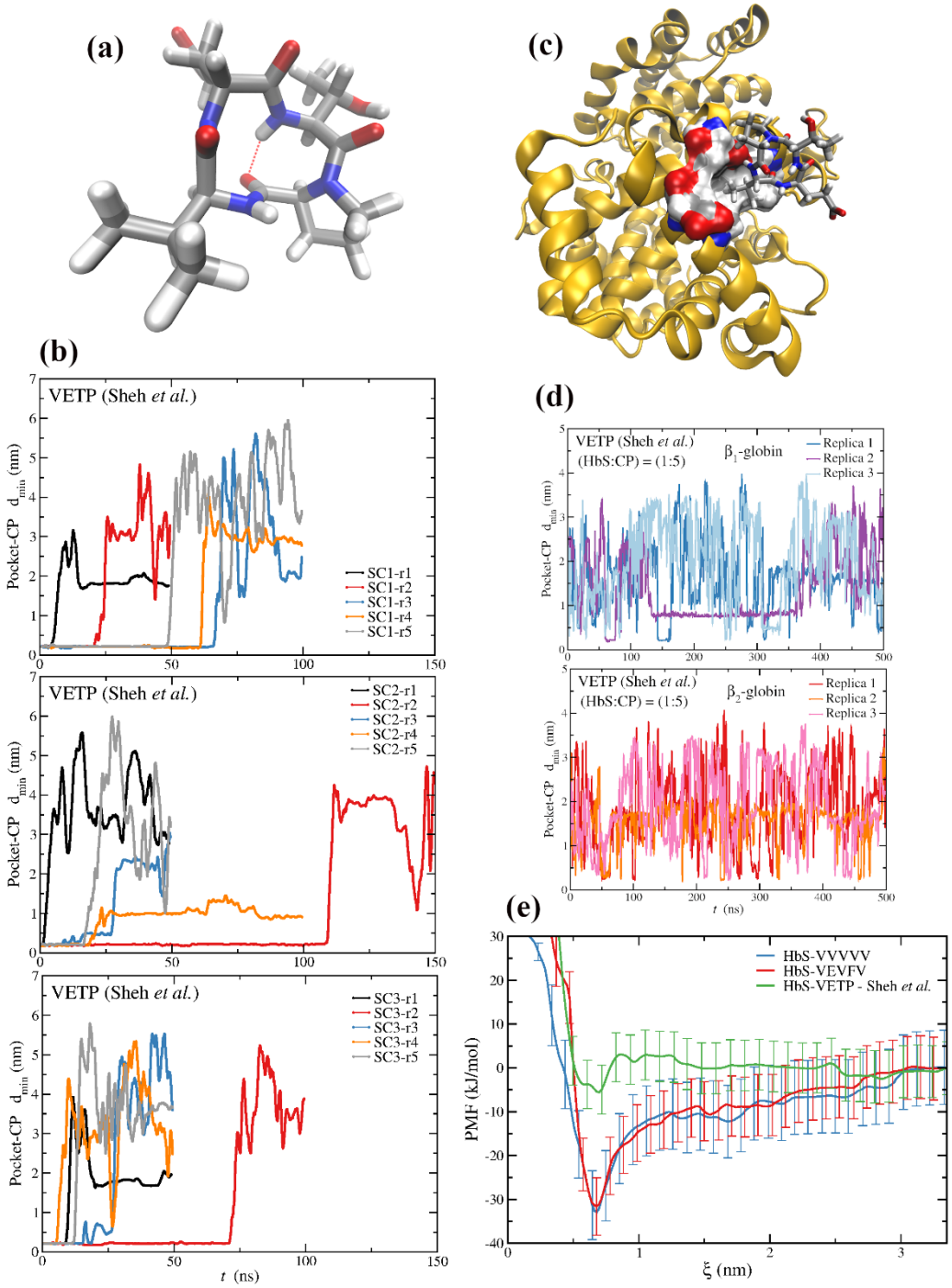

Figure 9 – **(a)** Density functional theory B3LYP/6-31+G(d,p) local minima for VETP; **(b)** Moving averages of the time evolution of the minimum distance between the VETP and the pocket up to a maximum residence time of 150 ns. SC stands for starting conformation (HbS-CP) and r stands for replicate. Five representative replicates are shown for each SC; **(c)** Representative configuration illustrating the relative orientation of VETP in the HbS pocket; **(d)** Moving averages of the time evolution of the minimum distance between five VETP and the β_1 and β_2-globin pockets from MD trajectories where the CPs are randomly inserted in solution at time zero; **(e)** Potential of mean force (PMF) for HbS:VVVVV, HbS:VEVFV, and HbS:VETP in water at 310 K and 0.1 MPa.

We also assessed the HbS-CP binding free energy for VETP as well as for VEVFV (the most promising CP according to **Table 1**) through umbrella sampling. **Figure 9(e)** shows that the binding free energy of VVVVV and VEVFV is lower (more negative) by a factor ~ 6 relative to VETP. Amongst the possible reasons underlying this discrepancy is the fact that VETP has a single Val, reducing the number of orientations the peptide can adopt to insert the Val-β6 side chain in the pocket. This should significantly reduce the CP specificity. Additionally, CP rotational motions can more easily result in unfavorable orientations, possibly explaining the shorter residence times and the much higher binding free energy. These results support, therefore, the promising application of some of the CPs proposed in this work as HbS nucleation blockers.

Conclusions and Perspectives

While new drugs have been recently approved for the treatment of SCD, none is always effective, and the development of new anti-sickling molecules remains of uttermost importance. Herein, we explored the possibility of using small macrocyclic peptides to block the hydrophobic pocket and/or its periphery, aiming to perturb the formation of lateral contacts underlying the aggregation process, while preserving the R-T equilibrium. Our results show that some hydrophobic and amphiphilic small CPs exhibit long residence times in the pocket. More strikingly, some of these CPs displayed a moderate to good specificity even at an HbS:CP (1:1) ratio. The CP orientation toward the pocket was found to be pivotal to the stabilization of the HbS-CP bound state, underlying many frustrated CP-pocket contacts. These contacts might, nevertheless, still delay or preclude the HbS aggregation process. Furthermore, hydration and binding free energies indicate that the CPs should be soluble in water. Overall, our results suggest that these molecules are promising HbS antisickling drug leads. Additional *in vitro* and *in vivo* studies are necessary to probe the real potential of these CPs, including their membrane permeability and selectivity capabilities. We expect such studies to be performed in a near future opening new avenues toward the design of effective anti-sickling CPs.

Acknowledgements

NG acknowledges financial support from Fundação para a Ciência e a Tecnologia (FCT) of Portugal (CEECIND/00821/2017). This work was supported by UIDB/04046/2020 and UIDP/04046/2020 centre grants from FCT, Portugal (to BioISI) and the Portuguese National Distributed Computing Infrastructure (http://www.incd.pt), and by the European Union (TWIN2PIPSA GA 101079147). Views and opinions expressed are, however, those of the author(s) only and do not necessarily reflect

those of the European Union or European Research Executive Agency (REA). Neither the European Union nor the granting authority can be held responsible for them.

Supporting Information

The following information is available free of charge:

Table 1 – Density, self-diffusion, and shear viscosity of the mTIP3P and TIP3P water models at 298 K and 0.1 MPas.
Figure S1 – RMSD and secondary structure of the CHARMM36 HbS model with the mTIP3P and TIP3P water models.
Figure S2 – Moving average of the minimum distance between the CP VVVVV and the HbS pocket in the HbS:CP (1:1) system, with the mTIP3P and TIP3P water models.
Figure S3 – Moving averages of the minimum distance between some CPs and the HbS pocket, up to 500 ns.
Figure S4 – Solvent accessible surface area (SASA) of the hydrophobic pocket involved in the lateral contact of HbS fibers.
Figure S5 - Normalized HbS-CP contact maps for the HbS:CP (1:1) systems for a R_{min} < 4.5 Å protein-CP contact definition.

References

(1) Pauling, L.; L, Itano, H. A.; Singer, S. J.; Wells, I. C. Sickle Cell Anemia, a Molecular Disease. *Science* **1949**, *110* (2865), 543.
(2) Ingram, V. M. A Specific Chemical Difference Between the Globins of Normal Human and Sickle-Cell Anæmia Hæmoglobin. *Nature* **1956**, *178* (4537), 792–794. https://doi.org/10.1038/178792a0.
(3) Ingram, V. M. Gene Mutations in Human Hæmoglobin: The Chemical Difference Between Normal and Sickle Cell Hæmoglobin. *Nature* **1957**, *180* (4581), 326–328. https://doi.org/10.1038/180326a0.
(4) Eaton, W. A.; Hofrichter, J. Sickle Cell Hemoglobin Polymerization. *Adv. Protein Chem.* **1990**, *40*, 63–279.
(5) Noguchi, C. T.; Schechter, A. N. Sickle Hemoglobin Polymerization in Solution and in Cells. *Annu. Rev. Biophys. Biophys. Chem.* **1985**, *14* (1), 239–263. https://doi.org/10.1146/annurev.bb.14.060185.001323.
(6) Dykes, G. W.; Crepeau, R. H.; Edelstein, S. J. Three-Dimensional Reconstruction of the 14-Filament Fibers of Hemoglobin S. *J. Mol. Biol.* **1979**, *130* (4), 451–472.
(7) Harrington, D. J.; Adachi, K.; Royer, W. E. The High Resolution Crystal Structure of Deoxyhemoglobin S. *J. Mol. Biol.* **1997**, *272* (3), 398–407. https://doi.org/10.1006/jmbi.1997.1253.
(8) Padlan, E. A.; Love, W. E. Refined Crystal Structure of Deoxyhemoglobin S I. Restrained Least-Squares Refinement at 3.0-8 Resolution. *J. Biol. Chem.* **1985**, *260* (14), 8272.
(9) Padlan, E. A.; Love, W. A. Refined Crystal Structure of Deoxyhemoglobin S II. Molecular Interactions in the Crystal. *J. Biol. Chem.* **1985**, *260* (14), 8280.
(10) Eaton, W. A.; Bunn, H. F. Treating Sickle Cell Disease by Targeting HbS Polymerization. *Blood* **2017**, *129* (20), 2719–2726. https://doi.org/10.1182/blood-2017-02-765891.
(11) Tisdale, J. F.; Thein, S. L.; Eaton, W. A. Treating Sickle Cell Anemia. *Science* **2020**, *367* (6483), 1198–1199. https://doi.org/10.1126/science.aba3827.
(12) Perutz, M. F. Stereochemistry of Cooperative Effects in Haemoglobin: Haem–Haem Interaction and the Problem of Allostery. *Nature* **1970**, *228* (5273), 726–734.

https://doi.org/10.1038/228726a0.
(13) Wishner, B. C.; Ward, K. B.; Lattman, E. E.; Love, W. E. Crystal Structure of Sickle-Cell Deoxyhemoglobin at 5 Å Resolution. *J. Mol. Biol.* **1975**, *98* (1), 179–194. https://doi.org/10.1016/S0022-2836(75)80108-2.
(14) Edelstein, S. J. Structure of the Fibers of Hemoglobin S. *Tex. Rep. Biol. Med.* **1980**, *40*, 221–232.
(15) Dykes, G.; Crepeau, R. H.; Edelstein, S. J. Three-Dimensional Reconstruction of the Fibres of Sickle Cell Haemoglobin. *Nature* **1978**, *272* (5653), 506–510. https://doi.org/10.1038/272506a0.
(16) Kato, G. J.; Piel, F. B.; Reid, C. D.; Gaston, M. H.; Ohene-Frempong, K.; Krishnamurti, L.; Smith, W. R.; Panepinto, J. A.; Weatherall, D. J.; Costa, F. F.; Vichinsky, E. P. Sickle Cell Disease. *Nat. Rev. Dis. Primer* **2018**, *4* (1), 18010. https://doi.org/10.1038/nrdp.2018.10.
(17) Wang, Y.; Ferrone, F. A. Dissecting the Energies That Stabilize Sickle Hemoglobin Polymers. *Biophys. J.* **2013**, *105* (9), 2149–2156. https://doi.org/10.1016/j.bpj.2013.09.032.
(18) Ferrone, F. A.; Hofrichter, J.; Eaton, W. A. Kinetics of Sickle Hemoglobin Polymerization. I. Studies Using Temperature-Jump and Laser Photolysis Techniques. *J. Mol. Biol.* **1985**, *183* (4), 591–610.
(19) Ferrone, F. A.; Hofrichter, J.; Eaton, W. A. Kinetics of Sickle Hemoglobin Polymerization. II. A Double Nucleation Mechanism. *J. Mol. Biol.* **1985**, *183* (4), 611–631.
(20) Ault, A. US FDA Approves First Drug for Sickle-Cell Anaemia. *The Lancet* **1998**, *351* (9105), 809. https://doi.org/10.1016/S0140-6736(05)78941-8.
(21) Cokic, V. P.; Smith, R. D.; Beleslin-Cokic, B. B.; Njoroge, J. M.; Miller, J. L.; Gladwin, M. T.; Schechter, A. N. Hydroxyurea Induces Fetal Hemoglobin by the Nitric Oxide–Dependent Activation of Soluble Guanylyl Cyclase. *J. Clin. Invest.* **2003**, *111* (2), 231–239. https://doi.org/10.1172/JCI200316672.
(22) Ortiz de Montellano, P. R. A New Step in the Treatment of Sickle Cell Disease: Published as Part of the *Biochemistry* Series "Biochemistry to Bedside." *Biochemistry* **2017**, *57* (5), 470–471. https://doi.org/10.1021/acs.biochem.7b00785.
(23) Niihara, Y.; Zerez, C. R.; Akiyama, D. S.; Tanaka, K. R. Oral L-Glutamine Therapy for Sickle Cell Anemia: I. Subjective Clinical Improvement and Favorable Change in Red Cell NAD Redox Potential. *Am. J. Hematol.* **1998**, *58* (2), 117–121. https://doi.org/10.1002/(SICI)1096-8652(199806)58:2<117::AID-AJH5>3.0.CO;2-V.
(24) Niihara, Y.; Zerez, C. R.; Akiyama, D. S.; Tanaka, K. R. Increased Red Cell Glutamine Availability in Sickle Cell Anemia: Demonstration of Increased Active Transport, Affinity, and Increased Glutamate Level in Intact Red Cells. *J. Lab. Clin. Med.* **1997**, *130* (1), 83–90.
(25) Niihara, Y.; Miller, S. T.; Kanter, J.; Lanzkron, S.; Smith, W. R.; Hsu, L. L.; Gordeuk, V. R.; Viswanathan, K.; Sarnaik, S.; Osunkwo, I.; Guillaume, E.; Sadanandan, S.; Sieger, L.; Lasky, J. L.; Panosyan, E. H.; Blake, O. A.; New, T. N.; Bellevue, R.; Tran, L. T.; Razon, R. L.; Stark, C. W.; Neumayr, L. D.; Vichinsky, E. P. A Phase 3 Trial of L -Glutamine in Sickle Cell Disease. *N. Engl. J. Med.* **2018**, *379* (3), 226–235. https://doi.org/10.1056/NEJMoa1715971.
(26) Vichinsky, E.; Hoppe, C. C.; Ataga, K. I.; Ware, R. E.; Nduba, V.; El-Beshlawy, A.; Hassab, H.; Achebe, M. M.; Alkindi, S.; Brown, R. C.; Diuguid, D. L.; Telfer, P.; Tsitsikas, D. A.; Elghandour, A.; Gordeuk, V. R.; Kanter, J.; Abboud, M. R.; Lehrer-Graiwer, J.; Tonda, M.; Intondi, A.; Tong, B.; Howard, J. A Phase 3 Randomized Trial of Voxelotor in Sickle Cell Disease. *N. Engl. J. Med.* **2019**, *381* (6), 509–519. https://doi.org/10.1056/NEJMoa1903212.
(27) Henry, E. R.; Metaferia, B.; Li, Q.; Harper, J.; Best, R. B.; Glass, K. E.; Cellmer, T.; Dunkelberger, E. B.; Conrey, A.; Thein, S. L.; Bunn, H. F.; Eaton, W. A. Treatment of Sickle Cell Disease by Increasing Oxygen Affinity of Hemoglobin. *Blood* **2021**, *138* (13), 1172–1181. https://doi.org/10.1182/blood.2021012070.
(28) Eapen, M.; Brazauskas, R.; Walters, M. C.; Bernaudin, F.; Bo-Subait, K.; Fitzhugh, C. D.;

Hankins, J. S.; Kanter, J.; Meerpohl, J. J.; Bolaños-Meade, J.; Panepinto, J. A.; Rondelli, D.; Shenoy, S.; Williamson, J.; Woolford, T. L.; Gluckman, E.; Wagner, J. E.; Tisdale, J. F. Effect of Donor Type and Conditioning Regimen Intensity on Allogeneic Transplantation Outcomes in Patients with Sickle Cell Disease: A Retrospective Multicentre, Cohort Study. *Lancet Haematol.* **2019**, *6* (11), e585–e596. https://doi.org/10.1016/S2352-3026(19)30154-1.

(29) Ribeil, J.-A.; Hacein-Bey-Abina, S.; Payen, E.; Magnani, A.; Semeraro, M.; Magrin, E.; Caccavelli, L.; Neven, B.; Bourget, P.; El Nemer, W.; Bartolucci, P.; Weber, L.; Puy, H.; Meritet, J.-F.; Grevent, D.; Beuzard, Y.; Chrétien, S.; Lefebvre, T.; Ross, R. W.; Negre, O.; Veres, G.; Sandler, L.; Soni, S.; de Montalembert, M.; Blanche, S.; Leboulch, P.; Cavazzana, M. Gene Therapy in a Patient with Sickle Cell Disease. *N. Engl. J. Med.* **2017**, *376* (9), 848–855. https://doi.org/10.1056/NEJMoa1609677.

(30) Kapoor, S.; Little, J. A.; Pecker, L. H. Advances in the Treatment of Sickle Cell Disease. *Mayo Clin. Proc.* **2018**, *93* (12), 1810–1824. https://doi.org/10.1016/j.mayocp.2018.08.001.

(31) Telen, M. J.; Malik, P.; Vercellotti, G. M. Therapeutic Strategies for Sickle Cell Disease: Towards a Multi-Agent Approach. *Nat. Rev. Drug Discov.* **2019**, *18* (2), 139–158. https://doi.org/10.1038/s41573-018-0003-2.

(32) Salinas Cisneros, G.; Thein, S. L. Recent Advances in the Treatment of Sickle Cell Disease. *Front. Physiol.* **2020**, *11*, 435. https://doi.org/10.3389/fphys.2020.00435.

(33) Martins, G.; Galamba, N. *Protein Aggregation-Inhibition: A Therapeutic Route from Parkinson's Disease to Sickle Cell Anemia*; preprint; Chemistry, 2023. https://doi.org/10.26434/chemrxiv-2023-glrmw.

(34) Dean, J.; Schechter, A. N. Sickle-Cell Anemia: Molecular and Cellular Bases of Therapeutic Approaches: (First of Three Parts). *N. Engl. J. Med.* **1978**, *299* (14), 752–763. https://doi.org/10.1056/NEJM197810052991405.

(35) Metaferia, B.; Cellmer, T.; Dunkelberger, E. B.; Li, Q.; Henry, E. R.; Hofrichter, J.; Staton, D.; Hsieh, M. M.; Conrey, A. K.; Tisdale, J. F.; Chatterjee, A. K.; Thein, S. L.; Eaton, W. A. Phenotypic Screening of the ReFRAME Drug Repurposing Library to Discover New Drugs for Treating Sickle Cell Disease. *Proc. Natl. Acad. Sci.* **2022**, *119* (40), e2210779119. https://doi.org/10.1073/pnas.2210779119.

(36) Olubiyi, O. O.; Olagunju, M. O.; Strodel, B. Rational Drug Design of Peptide-Based Therapies for Sickle Cell Disease. *Molecules* **2019**, *24* (24), 4551. https://doi.org/10.3390/molecules24244551.

(37) Noguchi, C. T.; Schechter, A. N. Inhibition of Sickle Hemoglobin Gelation by Amino Acids and Related Compounds. *Biochemistry* **1978**, *17* (25), 5455–5459. https://doi.org/10.1021/bi00618a020.

(38) Gorecki, M.; Votano, J. R.; Rich, A. Peptide Inhibitors of Sickle Hemoglobin Aggregation: Effect of Hydrophobicity. *Biochemistry* **1980**, *19* (8), 1564–1568. https://doi.org/10.1021/bi00549a005.

(39) Votano, J. R.; Rich, A. Inhibition of Deoxyhemoglobin S Polymerization by Biaromatic Peptides Found to Associate with the Hemoglobin Molecule at a Preferred Site. *Biochemistry* **1985**, *24* (8), 1966–1970. https://doi.org/10.1021/bi00329a025.

(40) Armiento, V.; Spanopoulou, A.; Kapurniotu, A. Peptide-Based Molecular Strategies To Interfere with Protein Misfolding, Aggregation, and Cell Degeneration. *Angew. Chem. Int. Ed.* **2020**, *59* (9), 3372–3384. https://doi.org/10.1002/anie.201906908.

(41) Neddenriep, B.; Calciano, A.; Conti, D.; Sauve, E.; Paterson, M.; Bruno, E.; A. Moffet, D. Short Peptides as Inhibitors of Amyloid Aggregation. *Open Biotechnol. J.* **2011**, *5* (1), 39–46. https://doi.org/10.2174/1874070701105010039.

(42) Cunningham, A. D.; Qvit, N.; Mochly-Rosen, D. Peptides and Peptidomimetics as Regulators of Protein–Protein Interactions. *Curr. Opin. Struct. Biol.* **2017**, *44*, 59–66. https://doi.org/10.1016/j.sbi.2016.12.009.

(43) Vinogradov, A. A.; Yin, Y.; Suga, H. Macrocyclic Peptides as Drug Candidates: Recent Progress and Remaining Challenges. *J. Am. Chem. Soc.* **2019**, *141* (10), 4167–4181. https://doi.org/10.1021/jacs.8b13178.
(44) Dougherty, P. G.; Sahni, A.; Pei, D. Understanding Cell Penetration of Cyclic Peptides. *Chem. Rev.* **2019**, *119* (17), 10241–10287. https://doi.org/10.1021/acs.chemrev.9b00008.
(45) Gentilucci, L.; De Marco, R.; Cerisoli, L. Chemical Modifications Designed to Improve Peptide Stability: Incorporation of Non-Natural Amino Acids, Pseudo-Peptide Bonds, and Cyclization. *Curr. Pharm. Des.* **2010**, *16* (28), 3185–3203. https://doi.org/10.2174/138161210793292555.
(46) Lipinski, C. A.; Lombardo, F.; Dominy, B. W.; Feeney, P. J. Experimental and Computational Approaches to Estimate Solubility and Permeability in Drug Discovery and Development Settings 1PII of Original Article: S0169-409X(96)00423-1. The Article Was Originally Published in Advanced Drug Delivery Reviews 23 (1997) 3–25. 1. *Adv. Drug Deliv. Rev.* **2001**, *46* (1–3), 3–26. https://doi.org/10.1016/S0169-409X(00)00129-0.
(47) Sheh, L.; Mokotoff, M.; Abraham, D. J. Design, Synthesis, and Testing of Potential Antisickling Agents. 9. Cyclic Tetrapeptide Homologs as Mimics of the Mutation Site of Hemoglobin S. *Int. J. Pept. Protein Res.* **1987**, *29* (4), 509–520. https://doi.org/10.1111/j.1399-3011.1987.tb02278.x.
(48) Galkin, O.; Pan, W.; Filobelo, L.; Hirsch, R. E.; Nagel, R. L.; Vekilov, P. G. Two-Step Mechanism of Homogeneous Nucleation of Sickle Cell Hemoglobin Polymers. *Biophys. J.* **2007**, *93* (3), 902–913. https://doi.org/10.1529/biophysj.106.103705.
(49) Samuel, R. E.; Salmon, E. D.; Briehl, R. W. Nucleation and Growth of Fibres and Gel Formation in Sickle Cell Haemoglobin. *Nature* **1990**, *345* (6278), 833–835. https://doi.org/10.1038/345833a0.
(50) Galamba, N.; Pipolo, S. On the Binding Free Energy and Molecular Origin of Sickle Cell Hemoglobin Aggregation. *J. Phys. Chem. B* **2018**, *122* (30), 7475–7483. https://doi.org/10.1021/acs.jpcb.8b03708.
(51) Galamba, N. On the Nonaggregation of Normal Adult Hemoglobin and the Aggregation of Sickle Cell Hemoglobin. *J. Phys. Chem. B* **2019**, *123* (50), 10735–10745. https://doi.org/10.1021/acs.jpcb.9b09727.
(52) Best, R. B.; Zhu, X.; Shim, J.; Lopes, P. E. M.; Mittal, J.; Feig, M.; MacKerell, A. D. Optimization of the Additive CHARMM All-Atom Protein Force Field Targeting Improved Sampling of the Backbone ϕ, ψ and Side-Chain χ_1 and χ_2 Dihedral Angles. *J. Chem. Theory Comput.* **2012**, *8* (9), 3257–3273. https://doi.org/10.1021/ct300400x.
(53) Huang, J.; MacKerell, A. D. CHARMM36 All-Atom Additive Protein Force Field: Validation Based on Comparison to NMR Data. *J. Comput. Chem.* **2013**, *34* (25), 2135–2145. https://doi.org/10.1002/jcc.23354.
(54) Jorgensen, W. L.; Chandrasekhar, J.; Madura, J. D.; Impey, R. W.; Klein, M. L. Comparison of Simple Potential Functions for Simulating Liquid Water. *J. Chem. Phys.* **1983**, *79* (2), 926–935. https://doi.org/10.1063/1.445869.
(55) Boonstra, S.; Onck, P. R.; Van Der Giessen, E. CHARMM TIP3P Water Model Suppresses Peptide Folding by Solvating the Unfolded State. *J. Phys. Chem. B* **2016**, *120* (15), 3692–3698. https://doi.org/10.1021/acs.jpcb.6b01316.
(56) Park, S.-Y.; Yokoyama, T.; Shibayama, N.; Shiro, Y.; Tame, J. R. H. 1.25 Å Resolution Crystal Structures of Human Haemoglobin in the Oxy, Deoxy and Carbonmonoxy Forms. *J. Mol. Biol.* **2006**, *360* (3), 690–701. https://doi.org/10.1016/j.jmb.2006.05.036.
(57) Becke, A. D. Density-functional Thermochemistry. III. The Role of Exact Exchange. *J. Chem. Phys.* **1993**, *98* (7), 5648–5652. https://doi.org/10.1063/1.464913.
(58) Stephens, P. J.; Devlin, F. J.; Chabalowski, C. F.; Frisch, M. J. Ab Initio Calculation of Vibrational Absorption and Circular Dichroism Spectra Using Density Functional Force Fields. *J. Phys. Chem.* **1994**, *98* (45), 11623–11627. https://doi.org/10.1021/j100096a001.

(59) Frisch, M. J.; et al. Gaussian 16, Revision C.01.
(60) Dougherty, P. G.; Qian, Z.; Pei, D. Macrocycles as Protein–Protein Interaction Inhibitors. *Biochem. J.* **2017**, *474* (7), 1109–1125. https://doi.org/10.1042/BCJ20160619.
(61) Bussi, G.; Donadio, D.; Parrinello, M. Canonical Sampling through Velocity Rescaling. *J. Chem. Phys.* **2007**, *126* (1), 014101. https://doi.org/10.1063/1.2408420.
(62) Parrinello, M.; Rahman, A. Polymorphic Transitions in Single Crystals: A New Molecular Dynamics Method. *J. Appl. Phys.* **1981**, *52* (12), 7182–7190. https://doi.org/10.1063/1.328693.
(63) Essmann, U.; Perera, L.; Berkowitz, M. L.; Darden, T.; Lee, H.; Pedersen, L. G. A Smooth Particle Mesh Ewald Method. *J. Chem. Phys.* **1995**, *103* (19), 8577–8593. https://doi.org/10.1063/1.470117.
(64) Kirkwood, J. G. Statistical Mechanics of Fluid Mixtures. *J. Chem. Phys.* **1935**, *3* (5), 300–313. https://doi.org/10.1063/1.1749657.
(65) Chandler, D. *Introduction to Modern Statistical Mechanics*; Oxford University Press: New York, 1987.
(66) Torrie, G. M.; Valleau, J. P. Nonphysical Sampling Distributions in Monte Carlo Free-Energy Estimation: Umbrella Sampling. *J. Comput. Phys.* **1977**, *23* (2), 187–199. https://doi.org/10.1016/0021-9991(77)90121-8.
(67) Torrie, G. M.; Valleau, J. P. Monte Carlo Free Energy Estimates Using Non-Boltzmann Sampling: Application to the Sub-Critical Lennard-Jones Fluid. *Chem. Phys. Lett.* **1974**, *28* (4), 578–581. https://doi.org/10.1016/0009-2614(74)80109-0.
(68) Kästner, J. Umbrella Sampling. *Wiley Interdiscip. Rev. Comput. Mol. Sci.* **2011**, *1* (6), 932–942. https://doi.org/10.1002/wcms.66.
(69) Kumar, S.; Rosenberg, J. M.; Bouzida, D.; Swendsen, R. H.; Kollman, P. A. The Weighted Histogram Analysis Method for Free-Energy Calculations on Biomolecules. I. The Method. *J. Comput. Chem.* **1992**, *13* (8), 1011–1021. https://doi.org/10.1002/jcc.540130812.
(70) Souaille, M.; Roux, B. Extension to the Weighted Histogram Analysis Method: Combining Umbrella Sampling with Free Energy Calculations. *Comput. Phys. Commun.* **2001**, *135* (1), 40–57. https://doi.org/10.1016/S0010-4655(00)00215-0.
(71) Neumann, R. M. Entropic Approach to Brownian Movement. *Am. J. Phys.* **1980**, *48* (5), 354–357. https://doi.org/10.1119/1.12095.
(72) Trzesniak, D.; Kunz, A.-P. E.; van Gunsteren, W. F. A Comparison of Methods to Compute the Potential of Mean Force. *ChemPhysChem* **2007**, *8* (1), 162–169. https://doi.org/10.1002/cphc.200600527.
(73) Hub, J. S.; de Groot, B. L.; van der Spoel, D. G_wham—A Free Weighted Histogram Analysis Implementation Including Robust Error and Autocorrelation Estimates. *J. Chem. Theory Comput.* **2010**, *6* (12), 3713–3720. https://doi.org/10.1021/ct100494z.
(74) Bennett, C. H. Efficient Estimation of Free Energy Differences from Monte Carlo Data. *J. Comput. Phys.* **1976**, *22* (2), 245–268. https://doi.org/10.1016/0021-9991(76)90078-4.
(75) Galamba, N. Aggregation of a Parkinson's Disease-Related Peptide: When Does Urea Weaken Hydrophobic Interactions? *ACS Chem. Neurosci.* **2022**, *13* (12), 1769–1781. https://doi.org/10.1021/acschemneuro.2c00169.
(76) Martins, G. F.; Nascimento, C.; Galamba, N. Mechanistic Insights on Polyphenols' Aggregation Inhibition of Alpha-Synuclein and Related Peptides. *ACS Chem. Neurosci.* **2023**.
(77) Copeland, R. A.; Pompliano, D. L.; Meek, T. D. Drug–Target Residence Time and Its Implications for Lead Optimization. *Nat. Rev. Drug Discov.* **2006**, *5* (9), 730–739. https://doi.org/10.1038/nrd2082.
(78) Pan, A. C.; Borhani, D. W.; Dror, R. O.; Shaw, D. E. Molecular Determinants of Drug–Receptor Binding Kinetics. *Drug Discov. Today* **2013**, *18* (13–14), 667–673. https://doi.org/10.1016/j.drudis.2013.02.007.
(79) Swinney, D. C. The Role of Binding Kinetics in Therapeutically Useful Drug Action. *Curr.*

Opin. Drug Discov. Devel. **2009**, *12* (1), 31–39.
(80) Lu, H.; Tonge, P. J. Drug–Target Residence Time: Critical Information for Lead Optimization. *Curr. Opin. Chem. Biol.* **2010**, *14* (4), 467–474. https://doi.org/10.1016/j.cbpa.2010.06.176.

Graphical Abstract